

## Quasi-biennial oscillation and tracer distributions in a coupled chemistry-climate model

Wenshou Tian,<sup>1</sup> Martyn P. Chipperfield,<sup>1</sup> Lesley J. Gray,<sup>2</sup> and Joseph M. Zawodny<sup>3</sup>

Received 9 November 2005; revised 18 May 2006; accepted 26 June 2006; published 17 October 2006.

[1] We have used a fully coupled chemistry-climate model (CCM), which generates its own wind and temperature quasi-biennial oscillation (QBO), to study the effect of coupling on the QBO and to examine the QBO signals in stratospheric trace gases, particularly ozone. Radiative coupling of the interactive chemistry to the underlying general circulation model tends to prolong the QBO period and to increase the QBO amplitude in the equatorial zonal wind in the lower and middle stratosphere. The model ozone QBO agrees well with Stratospheric Aerosol and Gas Experiment II and Total Ozone Mapping Spectrometer satellite observations in terms of vertical and latitudinal structure. The model captures the ozone QBO phase change near 28 km over the equator and the column phase change near  $\pm 15^\circ$  latitude. Diagnosis of the model chemical terms shows that variations in  $\text{NO}_x$  are the main chemical driver of the  $\text{O}_3$  QBO around 35 km, i.e., above the  $\text{O}_3$  phase change.

**Citation:** Tian, W., M. P. Chipperfield, L. J. Gray, and J. M. Zawodny (2006), Quasi-biennial oscillation and tracer distributions in a coupled chemistry-climate model, *J. Geophys. Res.*, 111, D20301, doi:10.1029/2005JD006871.

### 1. Introduction

[2] Equatorial stratospheric winds and temperatures are observed to exhibit a downward propagating oscillating pattern with an average period of just over 2 years, known as the quasi-biennial oscillation (QBO). Both observational and modeling studies have found that QBO signals also exist in both short-lived and long-lived stratospheric chemical species such as  $\text{O}_3$ ,  $\text{NO}_2$  and  $\text{N}_2\text{O}$  [e.g., Gray and Pyle, 1989; Gray and Chipperfield, 1990; Zawodny and McCormick, 1991; Chipperfield and Gray, 1992; Chipperfield *et al.*, 1994; Randel and Wu, 1996; Baldwin *et al.*, 2001].

[3] Reed [1964] proposed that the QBO-induced meridional circulation could drive a QBO in total column ozone. During a descending easterly phase (i.e., winds from the east) there is an induced upwelling at the equator in the lower stratosphere so that the accompanying adiabatic cooling can maintain thermal wind balance. This upwelling results in a negative anomaly in column ozone at the equator since ozone increases with height in this region and hence there is anomalous advection of ozone-poor air from below. There is a return arm of this induced circulation in the subtropics producing a positive column ozone anomaly at these latitudes. During a descending westerly QBO phase the circulation is reversed, producing a positive column ozone anomaly at the equator and negative anomalies in the

subtropics. Gray and Pyle [1989] achieved the first simulation of the  $\text{O}_3$  QBO in a fully coupled 2D model and confirmed that the lower stratosphere  $\text{O}_3$  QBO is mainly controlled by transport processes. This was subsequently confirmed by 3D model simulations [e.g., Nagashima *et al.*, 1998].

[4] In addition to this dynamically induced QBO signal, Ling and London [1986], using a 1D photochemical model, proposed that the  $\text{O}_3$  QBO in the middle to upper stratosphere is forced directly by the temperature oscillation since ozone is largely under photochemical control above  $\sim 28$  km. Using a 2D model, Chipperfield *et al.* [1994] argued that the QBO modulation of  $\text{NO}_2$  is an important contributor of the QBO signal in  $\text{O}_3$  above 30 km, in addition to the temperature influence identified by Ling and London [1986]. Butchart *et al.* [2003], however, found from their 3D coupled chemistry-climate model (CCM) simulations, in which the  $\text{O}_3$  was fully interactive with radiative and dynamical fields, that an  $\text{O}_3$  QBO can be obtained without QBO-induced variations in  $\text{NO}_y$  transport and suggested therefore that ozone transport is important in forcing the ozone QBO in both the middle and lower stratosphere. It is apparent from these studies that the potential impacts of the QBO in zonal wind and temperature on global tracer transport and distributions need further investigation.

[5] The diabatic effect of chemical species' QBO signals on the temperature and wind oscillation is also still an issue of much debate. Hasebe [1994] argued that the diabatic effect of the ozone QBO through solar heating has a significant effect on the QBO-induced meridional circulation. Similarly, Li *et al.* [1995] found that diabatic heating due to the ozone QBO enhanced their modelled temperature QBO anomaly by 25%. However, in a similar 2D model study, Huang [1996] found that this effect was negligible.

<sup>1</sup>Institute for Atmospheric Science, School of Earth and Environment, University of Leeds, Leeds, UK.

<sup>2</sup>Centre for Global Atmospheric Modeling, Department of Meteorology, University of Reading, Reading, UK.

<sup>3</sup>NASA Langley Research Center, Hampton, Virginia, USA.

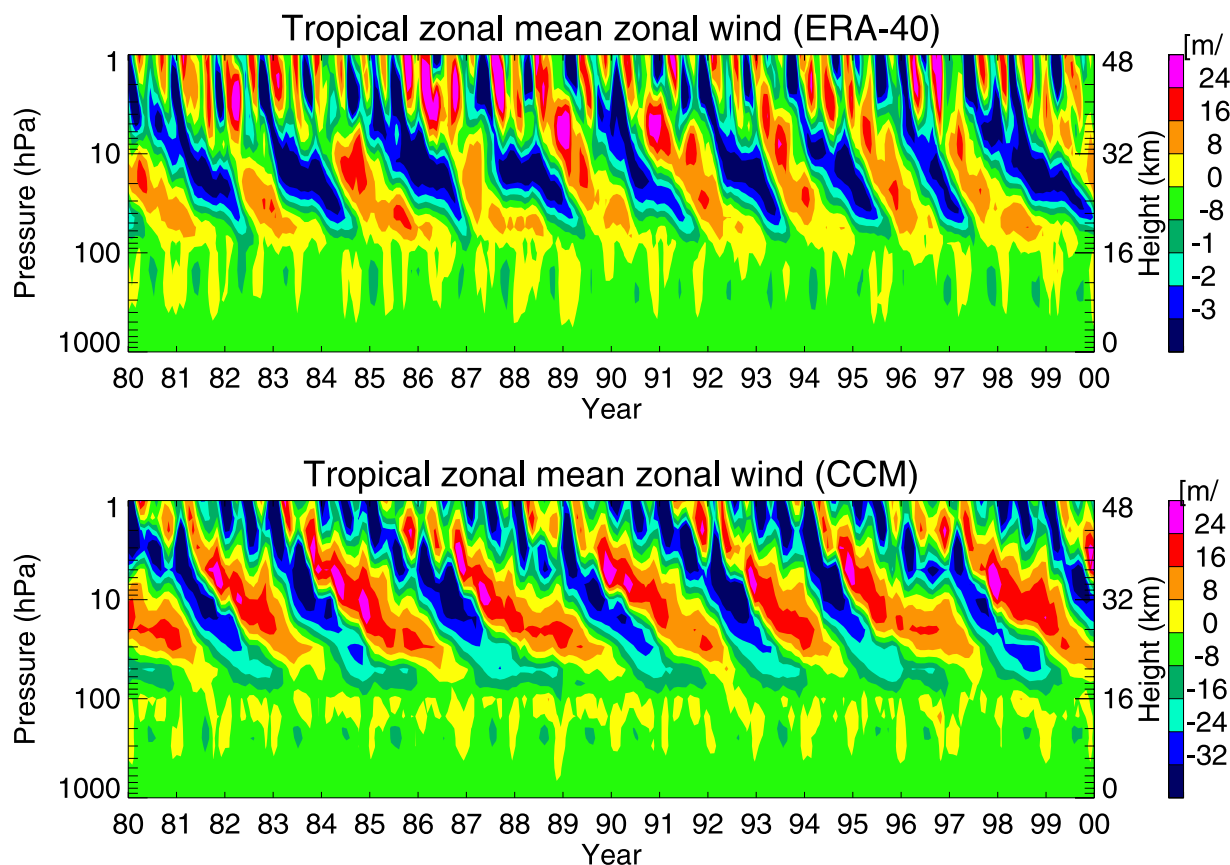


**Figure 1.** Height-time section of the QBO in the zonal mean zonal winds ( $\text{m s}^{-1}$ ) over the equator in (top) the ERA-40 data and (bottom) the coupled model simulation. The data are shown for a period of 20 years from 1980 to 2000.

[6] In most earlier studies, the dynamical processes were described in a 2D framework and the chemical processes were relatively simple. *Butchart et al.* [2003] pointed out that a better representation of chemical and dynamical processes in general circulation models (GCMs) will help to improve the interannual variability in climate models. In recent years, some GCMs have been able to produce QBO-like variations in the tropical zonal wind and these have been used to study the ozone QBO [e.g., *Bruhwyler and Hamilton*, 1999; *Butchart et al.*, 2003]. Nevertheless, those CCM studies have mainly focused on the ozone QBO and the treatment of the chemistry in their models is still relatively simplified.

[7] The motivation behind this study is to use a state-of-the-art GCM coupled with a comprehensive stratospheric chemistry scheme to investigate the QBO in chemical species and their interaction with the wind and temperature oscillations. We compare the model QBO signals of  $\text{O}_3$  with Stratospheric Aerosol and Gas Experiment II (SAGE II) and Total Ozone Mapping Spectrometer (TOMS) satellite data. The effects of chemistry coupling on the QBO are also investigated and the role of chemical processes in driving the ozone QBO is diagnosed. Section 2 describes our coupled model. Section 3 compares the modelled QBO in the equatorial zonal wind and temperature with observations. Section 4 discusses the impact of coupled chemistry on the equatorial zonal wind QBO. Sections 5 and 6 analyze the modelled QBO in  $\text{O}_3$ , and in  $\text{NO}_x$  and  $\text{NO}_y$ , respectively. Section 7 gives our summary and conclusions.

## 2. Model Description and Experiments

[8] The CCM used in this study is based on the troposphere-stratosphere-mesosphere version of the Met Office Unified Model (UM) [*Cullen*, 1993; *Swinbank et al.*, 1998] with a latitude-longitude resolution of  $2.5^\circ \times 3.75^\circ$ . The model has 64 vertical levels extending from the surface to 0.01 hPa ( $\sim 80$  km) with a resolution between 150 and 0.1 hPa (14.5 to 52.2 km) of about 1.5 km. It includes the *Warner and McIntyre* [1999] parameterization of gravity waves and therefore generates a QBO-like oscillation in equatorial winds and temperatures, as described by *Scaife et al.* [2000].

[9] The stratospheric chemistry scheme is from the established SLIMCAT/TOMCAT chemical transport model [*Chipperfield*, 1999]. The coupled model advects 28 tracers and includes 42 chemical species from the  $\text{O}_x$ ,  $\text{HO}_x$ ,  $\text{Cl}_y$ ,  $\text{Br}_y$ , and  $\text{NO}_y$  families and source gases. The model includes both gas phase chemistry and heterogeneous chemistry on liquid and solid aerosols and polar stratospheric clouds (PSCs). The  $\text{O}_3$ ,  $\text{N}_2\text{O}$ ,  $\text{CH}_4$  and  $\text{H}_2\text{O}$  fields are coupled to the UM's radiation scheme. The chemistry is calculated on 30 levels from  $\sim 150$  hPa to 0.5 hPa. A more detailed description of the CCM is provided by *Tian and Chipperfield* [2005].

[10] A control run of the fully coupled model was integrated for 21 years from 1979 to 2000 with time varying greenhouse gas (GHG) concentrations in the model's chemistry and radiation scheme. The model was first spun up for

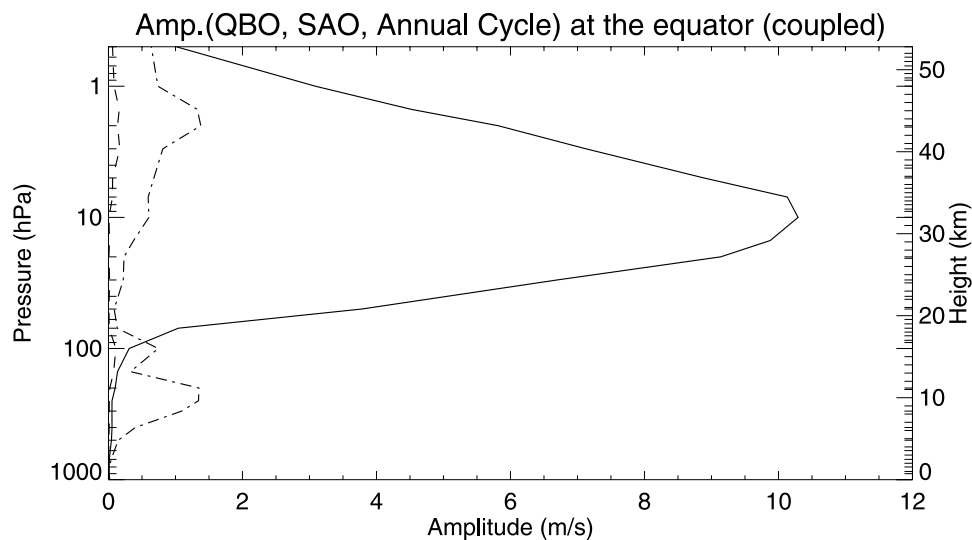


**Figure 2.** Vertical profiles of Fourier amplitude ( $\text{m s}^{-1}$ ) of the model annual cycle (dash-dotted line), QBO (solid line), and SAO (dashed line) at the equator. All amplitudes were calculated using the same method as that of *Pascoe et al.* [2005].

three years with fixed GHGs at 1978 values and then restarted. The sea surface temperatures (SSTs) and sea ice are from the Atmospheric Model Intercomparison Project II (AMIP II [see *Gates et al.*, 1999]) and the concentrations of GHGs used in the model simulations follow the IPCC A2 scenario [World Meteorological Organization, 2003]. The lower boundary conditions of  $\text{N}_2\text{O}$ ,  $\text{CH}_4$ , CFC11, and CFC12 in the chemistry scheme are updated monthly according to this A2 scenario and the concentrations of  $\text{CO}_2$ , CFC11, and CFC12 in the radiation scheme are updated year-by-year accordingly.

[11] We note that the version of the UM employed here is physically and dynamically similar to that of *Butchart et al.* [2003]. However, the chemistry scheme in their coupled model advects only 12 chemical tracers and the concentrations of long-lived species and families including  $\text{H}_2\text{O}$ ,  $\text{CH}_4$ ,  $\text{H}_2\text{SO}_4$ ,  $\text{Cl}_y$ ,  $\text{Br}_y$ , and  $\text{NO}_y$  were obtained by interpolating between zonal mean values specified for each month. In our model, those long-lived chemical species are all advected by the model with four of them coupled to the model radiation scheme.

### 3. QBO in Tropical Zonal Wind and Temperature

[12] Figure 1 shows the time series of the equatorial zonal winds from the European Centre for Medium-Range Weather Forecasts (ECMWF) ERA-40 reanalysis data and from the model simulation of our coupled chemistry run for the period of 1980–2000. The QBO signals are clearly seen in the model simulation. The maximum easterlies and westerlies are  $-35 \text{ m s}^{-1}$  and  $25 \text{ m s}^{-1}$ , respectively, while the temperature anomalies associated with the QBO are about  $\pm 4 \text{ K}$  (not shown). These values are comparable to values in the ERA-40 reanalyses [Pascoe et al., 2005]. The period of the simulated QBO is approximately 30 months, slightly longer than observed. We note that although the simulation used observed values of SSTs and GHGs for the period 1979–2000, the period of the QBO is not imposed and the small difference between simulated and observed QBO period

means that they are out of phase by the end of the time period. The QBO does not penetrate deep enough in the lower stratosphere compared with those in the ERA-40 data. *Scaife et al.* [2002] also found this and suggested it might be due to too much diffusion in the model at those lower levels. As shown by *Pascoe et al.* [2005] the zonal wind QBO signals in ERA-40 data extend down to a level of 100 hPa while in our model they only reach around 90 hPa. *Gray et al.* [2001] found from rocketsonde data that the tropical zonal wind is dominated by the semiannual oscillation (SAO) above 5 hPa and this is also evident in Figure 4d of *Pascoe et al.* [2005]. In our model, however, while there is evidently an oscillation of  $\sim 6$  month period around the height of the SAO between 1 and 10 hPa, the winds do not change sign every 6 months as in the observations. Instead, the sign change occurs on the QBO frequency, suggesting that the amplitude of the QBO is too strong at the upper levels. This is confirmed by Figure 2, which shows profiles of the amplitude of the model annual cycle, QBO and SAO at the equator. The amplitudes of the QBO and annual cycle are good compared with ERA-40 data but the amplitude of the SAO is too small.

### 4. Impact of Coupling on Zonal Wind QBO

[13] To identify the potential effects of radiative coupling on the equatorial wind QBO, another UM run without radiative coupling was performed. A climatology of the monthly ozone from the control run was calculated, ensuring an equal number of QBO east and west years, so that there was no QBO bias in the climatological fields. These monthly climatologies were then used repeatedly in the radiation scheme of the uncoupled run in order to eliminate the effect of the ozone QBO on the radiative heating. In this uncoupled run, which did not include the full chemistry module,  $\text{N}_2\text{O}$ ,  $\text{CH}_4$ , CFC11, and CFC12 values in the radiation scheme were kept constant with time (at 1990 values) but  $\text{CO}_2$  varied in the same way as in the control run.

[14] Figure 3 gives the Fourier spectrum of the zonal mean zonal wind time series over the equator calculated from the

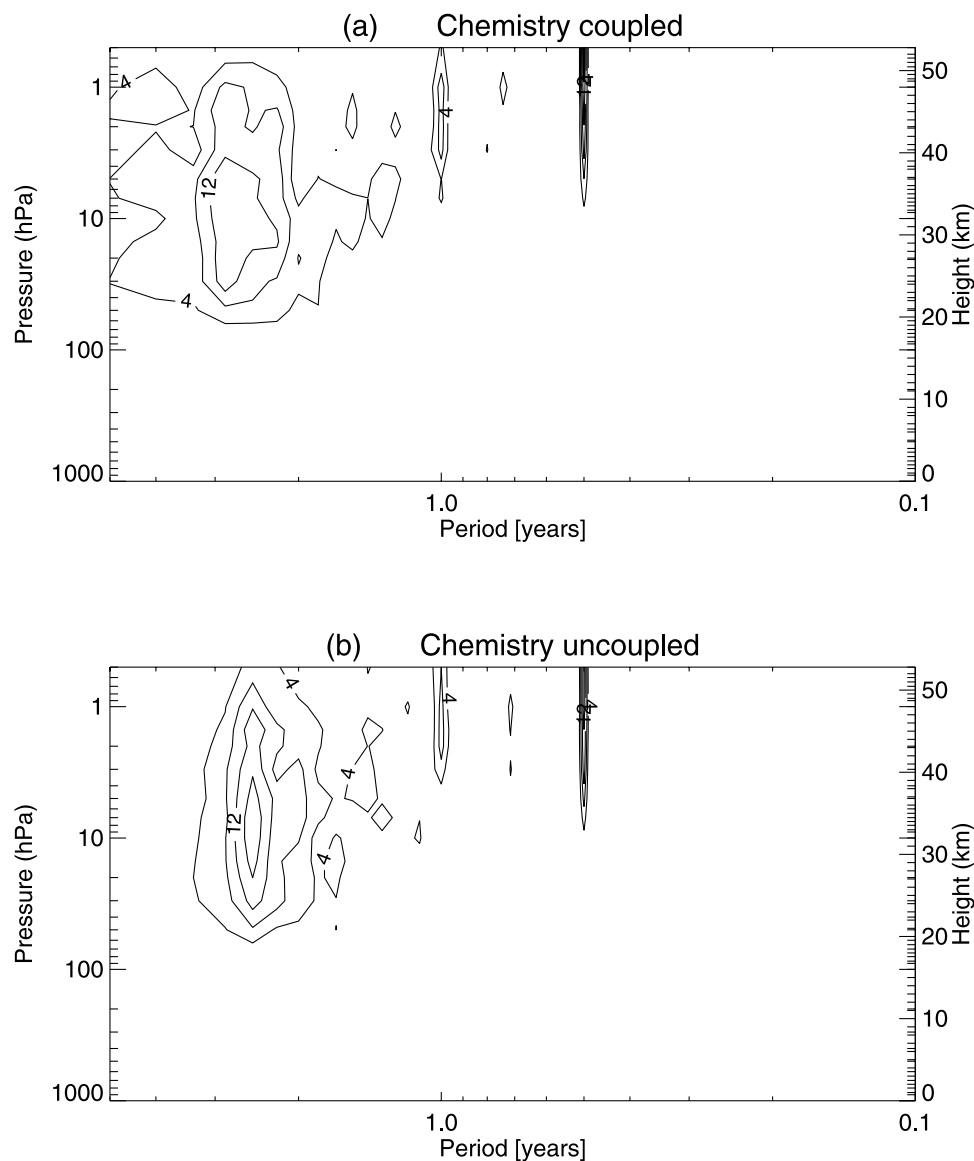


**Figure 3.** Fourier spectrum of the model equatorial zonal mean zonal wind for (a) the coupled run and (b) the uncoupled run. The Fourier frequency analysis was performed for each model level. The contours are drawn at the Fourier amplitudes of 1, 2, 4, 8, and 12  $\text{m s}^{-1}$ .

coupled and uncoupled model runs for the period 1980–2000. The most distinct mode of variability in both runs is the SAO with a period of 0.5 years. It extends down to  $\sim 7$  hPa in good agreement with *Pascoe et al.* [2005, Figure 3]. The annual signal is also evident in the upper stratosphere with the maximum frequency response near 1 hPa ( $\sim 45$  km) although, unlike the ERA-40 analysis, it does not penetrate to the lower stratosphere. There is no strong peak at any particular frequency in the QBO signal but a rather broad area of QBO sidebands, in good agreement with the ERA-40 data [*Pascoe et al.*, 2005] but the amplitudes are too strong, especially in the upper stratosphere.

[15] The effect of the coupling of the chemistry on the QBO frequency is evident. The amorphous QBO zone in the coupled run (Figure 3a) is broader with a more significant vertical variation than in the uncoupled run. The distinct maximum of the QBO frequency in the coupled run is about

2.5 years compared to about 2.2 years in the uncoupled run. This suggests that the diabatic effect of chemistry coupling prolongs the QBO period. *Butchart et al.* [2003] also found that the coupling of  $\text{O}_3$  chemistry to their GCM gave rise to a statistically significant increase of about 3 months in the mean period of the QBO. In our simulations, the increase in the QBO period due to chemistry feedback is even more significant with a 4-month increase within 20 years of simulation. A one-tailed  $t$  test based on 50, 20, and 5 hPa winds shows that the two simulations differ significantly at the 90% confidence level at least. This radiative/dynamical coupling is likely to be dominated by the  $\text{O}_3$  feedbacks rather than  $\text{H}_2\text{O}$  or the GHGs  $\text{CH}_4$  and  $\text{N}_2\text{O}$ . Changes in  $\text{O}_3$  affect both the absorption of solar radiation and of outgoing infrared radiation which will then affect the model temperature QBO. In turn, this can then affect the rates of chemical reactions and feedback on  $\text{O}_3$ . Note that temperature changes due to

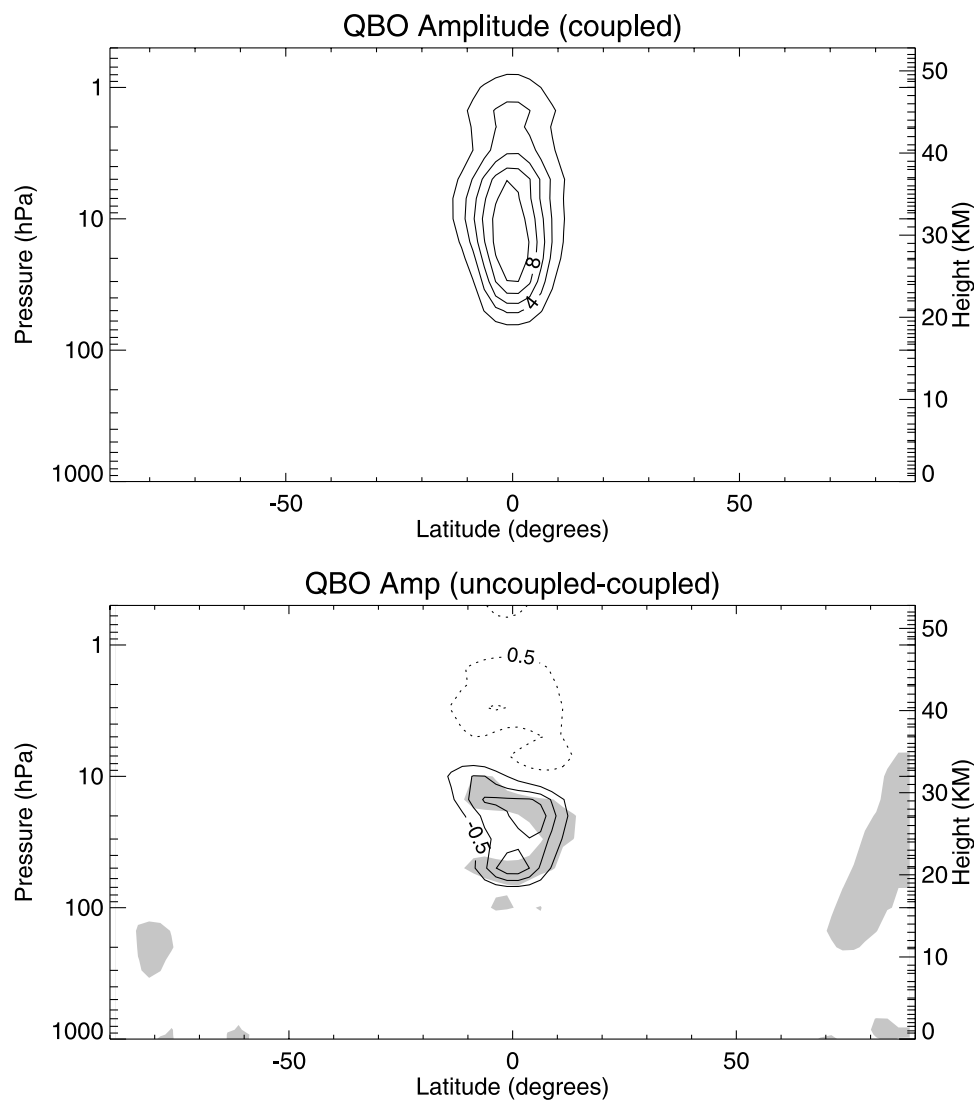


**Figure 4.** (top) Amplitudes of the QBO zonal mean zonal wind calculated using Fourier analysis from the coupled run. The contour interval is  $2 \text{ m s}^{-1}$ . (bottom) Differences in the Fourier amplitudes between the uncoupled and coupled runs (i.e., uncoupled minus coupled). The contours are  $\pm 0.5$ ,  $\pm 1.0$ , and  $\pm 1.5 \text{ m s}^{-1}$ . Regions where the variance of two time series differ significantly at the 90% level on the basis of an  $F$  statistic test are shaded.

coupling can also feedback on to  $\text{O}_3$  by impacting the dynamics.

[16] Figure 4 shows the Fourier amplitude of the zonal mean zonal wind time series obtained from the coupled run. The definition of the QBO amplitude is similar to that of Pascoe *et al.* [2005], i.e., the ratio of the power spectrum of the QBO to the power spectrum of the whole model data set. The QBO amplitude is therefore the sum of the squares of the amplitudes of the QBO harmonics 5–11 (for our 20-year time series) divided by the sum of the squares of all the harmonics. Also shown are the differences in the amplitudes between the coupled run and uncoupled run. The power of the QBO harmonics 5–11 accounts for a maximum 44% of the total power centered around 21 km in the coupled run, and a maximum contribution of 41% centered at 24 km in the uncoupled run. The QBO amplitude is increased by  $1.5 \text{ m s}^{-1}$  (17%) in the middle and lower stratosphere, and slightly

decreased by  $0.5 \text{ m s}^{-1}$  in the upper stratosphere, and is likely due to the chemistry coupling. An  $F$  statistic test indicates that the variances of the time series in the tropical middle and lower stratosphere differ significantly at the 90% confidence level between the coupled and uncoupled run.

[17] The maximum increase in the Fourier amplitude in the temperature QBO is about 0.8 K (not shown). This confirms the 2D model results of Li *et al.* [1995] and agrees well with the 3D model results of Butchart *et al.* [2003] who found that the diabatic effects of the ozone QBO increased the amplitude of the temperature oscillation by 35% ( $\sim 0.8 \text{ K}$ ).

[18] Figure 5 shows the monthly averaged equatorial zonal mean zonal wind shear between 30 and 50 hPa and the monthly averaged equatorial zonal mean temperature anomalies (from the climatological average) on the 30 hPa level in both runs. The temperature anomalies are around  $\pm 3 \text{ K}$ , about 1 K smaller than observed values derived from temperature

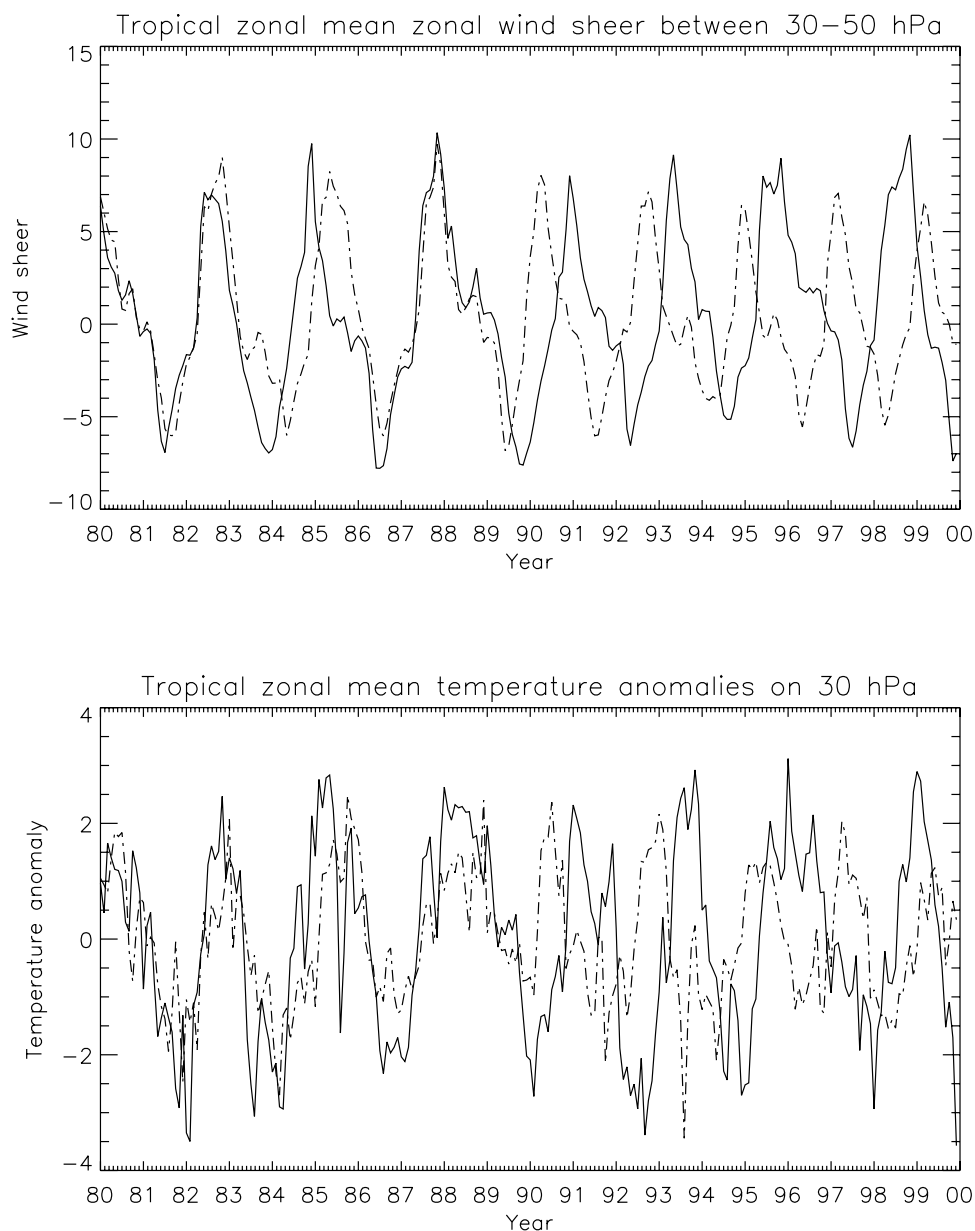


**Figure 5.** (top) Equatorial zonal mean vertical wind shear ( $\text{m s}^{-1} \text{km}^{-1}$ ) within 30–50 hPa layer and (bottom) deseasonalized temperature anomalies (K) for the period 1980–2000 at 30 hPa. The dash-dotted lines show the uncoupled model run, and the solid lines show the coupled model run.

measurements at Singapore [Baldwin *et al.*, 2001]. The wind shear between 30–50 hPa, which, as expected, is in phase with the temperature anomalies, is approximately  $\pm 8 \text{ m s}^{-1} \text{km}^{-1}$ , about  $2 \text{ m s}^{-1} \text{km}^{-1}$  larger than in ERA-40 data [Pascoe *et al.*, 2005]. Figure 5 also clearly shows that the coupling of chemistry to the GCM prolongs the period of the QBO signal.

## 5. Ozone QBO

[19] In this section we investigate the model's QBO signal in  $\text{O}_3$  and compare this with observations, principally from SAGE II (version 6.2). Although the model  $\text{O}_3$  QBO signal can be easily seen from the deseasonalized fields from the control run (not shown), to allow a more quantitative com-

parison of the general QBO structure with observations, both SAGE II data and the model output are first analyzed by the linear least squares regression analysis of Zawodny and McCormick [1991]. In this, the original SAGE II time series are fitted with a linear term and periodic terms of 4, 6, 9, 12, 18, 24, 30, 36 months. Then, the QBO signals are obtained by adding the terms with periods of 18, 24, and 30 months. For this study the SAGE II data have been extracted at a  $2.5^\circ$  latitude resolution with a  $10^\circ$  spatial smoothing. Note that the SAGE II data within the period 1991–1994 are not robust because of Mt. Pinatubo aerosol interferences. However, the intent of the CCM run is not to replicate the detailed SAGE II record but rather to demonstrate that the model produces a similar general structure of the QBO in chemical species. We do not expect to be able to directly compare the observations

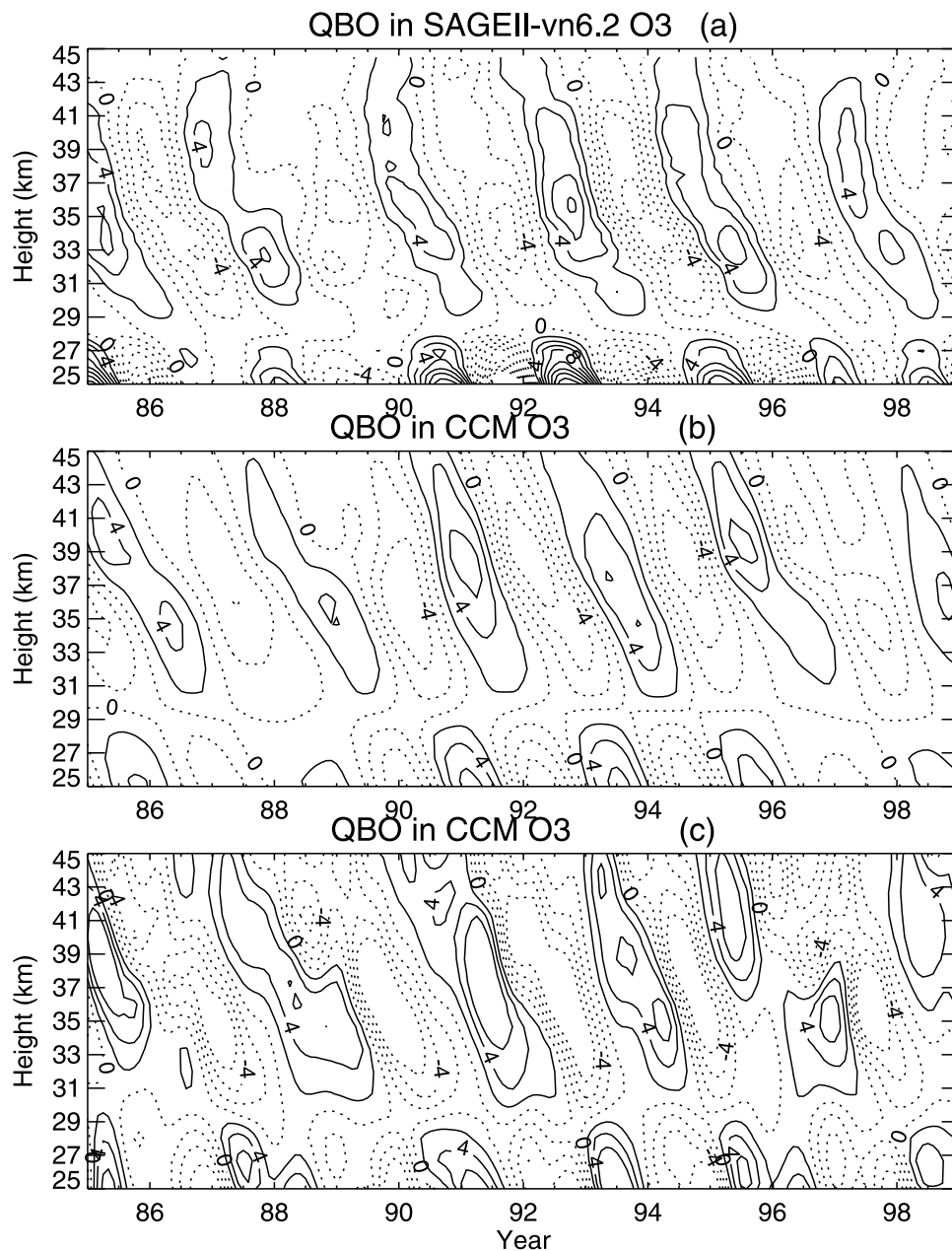


**Figure 6.** Height-time cross section of percentage anomaly in  $O_3$  at the equator from (a) SAGE II data and (b and c) the coupled model simulation. In Figure 6b the model output was analyzed in the same way as the SAGE II data (see text). In Figure 6c the output was analyzed using a 9–48 month digital band-pass filter. Contour interval is 4%; negative contours are dashed. The model pressure levels are converted to height levels by  $z = 16 \log(1000/p)$ , where  $p$  is pressure in hPa and  $z$  is height in km.

and the model simulations because of differences in timing and period of the QBO.

### 5.1. Time Series

[20] Figure 6 shows the percentage anomalies at the equator in SAGE II  $O_3$  and the  $O_3$  field from the fully coupled model run. (The anomaly here is the difference between a value in a detrended time series and the corresponding monthly mean value averaged over the whole time series.) Consistent with earlier analyses of SAGE II data, which showed a phase change in the anomaly at around 28–30 km [Zawodny and McCormick, 1991; Chipperfield et al.,

1994; Randel and Wu, 1996]. Figure 6 shows a phase change at around 28–30 km in both SAGE II data and the model simulations. Although slight differences in the QBO amplitude in the lower stratosphere exist between the model and observations, Figure 6 indicates that both the period and magnitude of the  $O_3$  QBO signal have been well reproduced by the model.

[21] We note that the choice of periods in this method of extracting the QBO signal is subjective and is not consistent with the method employed to quantify the QBO amplitude in Figure 4. However, it is a more appropriate method when dealing with data that has missing values and this is why it

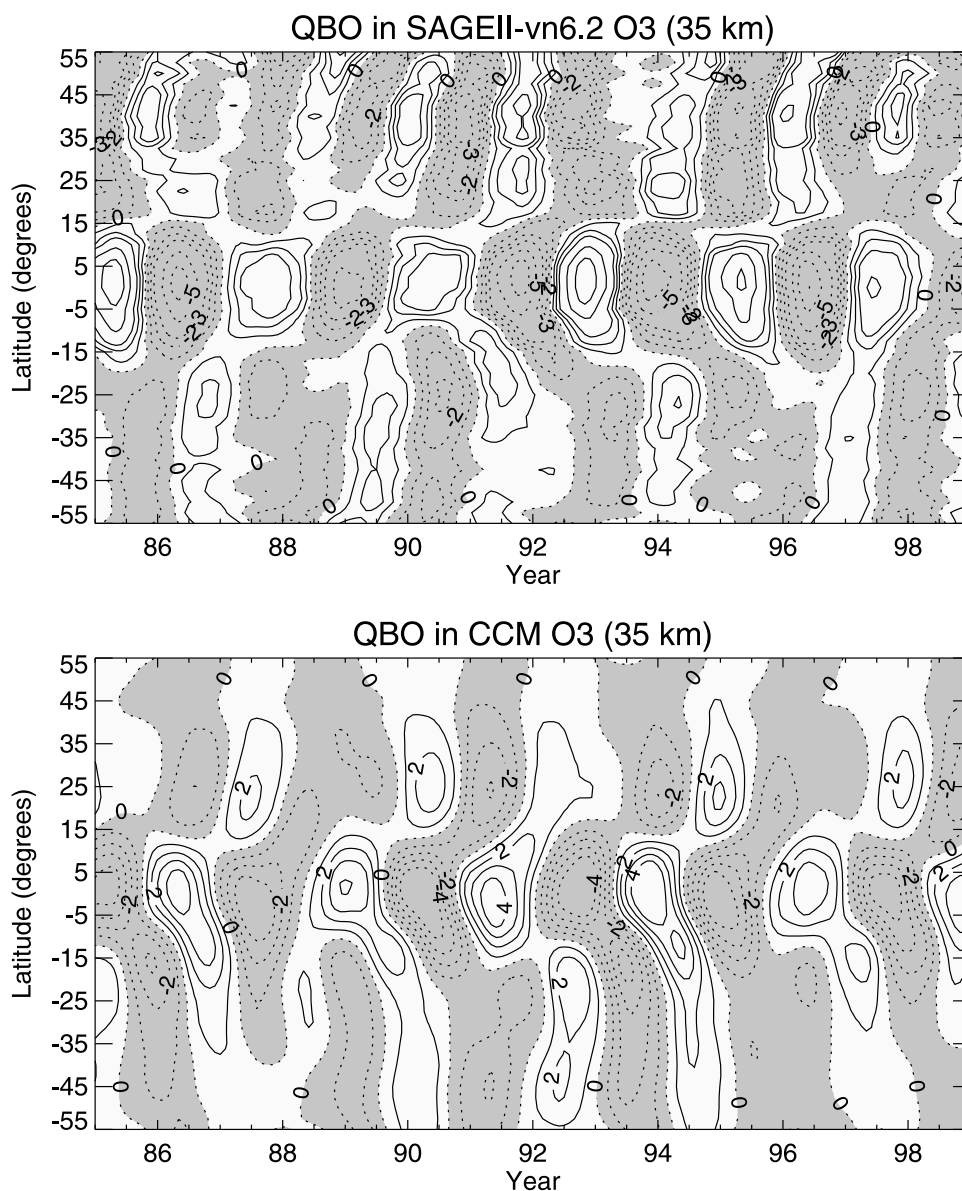


**Figure 7.** Latitude-time section of percentage anomaly in  $O_3$  at 35 km from (top) SAGE II data and (bottom) the coupled model simulation. Contour interval is 1%. Regions of negative anomalies are shaded.

was chosen to analyze the SAGE II data set. The CCM time series are continuous and hence the bandpass filtering technique employed by *Pascoe et al.* [2005] can be used here. In order to check that the results have not been compromised by the analysis technique, Figure 6c shows the time series of the ozone QBO extracted by applying a 9–48 month digital band-pass filter as done by *Pascoe et al.* [2005]. There are small differences in the details, such as the shape of the positive anomaly in 1996–1997, but the essential properties such as the period and phase change at  $\sim 29$  km are unaltered.

## 5.2. Latitude-Height Sections

[22] Figure 7 shows the latitudinal distribution of the  $O_3$  anomaly for SAGE II and the model at 35 km which is the approximate height of the maximum amplitude in the SAGE analysis. The magnitude of the model equatorial  $O_3$  QBO is of the same order as observed. The QBO signals at subtropical latitudes can be seen in both the SAGE II data and the

model simulation and the magnitudes of the signals are also consistent with each other. The modelled subtropical phase change occurs at around  $\pm 15^\circ$ , in agreement with the observations. The 2D simulations of *Chipperfield et al.* [1994] showed that the modelled subtropical phase changes are at around  $\pm 15^\circ$ . However, in their analysis of an earlier version of SAGE II (v5.9) data at a lower resolution, the subtropical phase change occurred near  $\pm 18^\circ$ . (If we analyze the SAGE II data with a resolution of  $5^\circ$  we also get a phase change near  $\pm 18^\circ$ ). At 25 km we find that the SAGE II phase change is near  $\pm 25^\circ$  but our modelled phase change is still near  $\pm 15^\circ$  (not shown). This discrepancy may be due to the inaccuracy of the fits of the SAGE II data in the lower stratosphere.

## 5.3. Column Ozone

[23] The QBO signals in the total column ozone from the model and TOMS observations [http://code916.gsfc.nasa.gov/data\\_services/index.html](http://code916.gsfc.nasa.gov/data_services/index.html) are shown in Figure 8. For

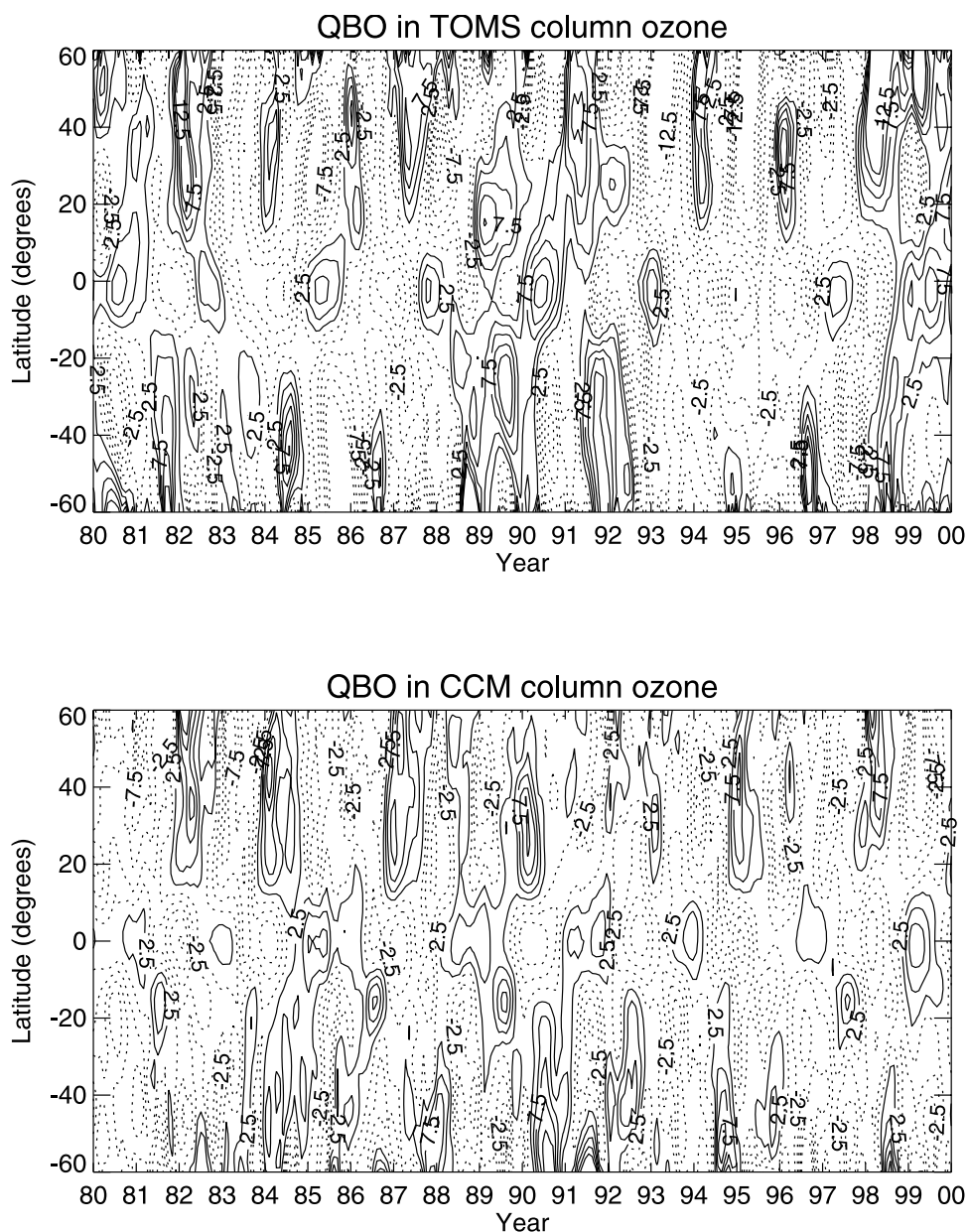


**Figure 8.** Latitude-time section of deseasonalized total column ozone anomalies (Dobson units, 1 DU = 0.001 atm cm) calculated from (top) TOMS data and (bottom) the coupled model simulation. Contour interval is 2.5 DU.

comparison with previous studies of models versus TOMS, the data have been deseasonalized with the linear trend removed, but with no filtering to bandpass the QBO frequencies. This results in a more noisy plot than for the SAGE II comparison. In the equatorial and southern subtropics, the modelled QBO signals are weaker in magnitude than observed while in the northern subtropics, the amplitude of the modelled QBO agrees overall with the observations. *Butchart et al.* [2003] pointed out that one weakness of their model is the lack of any discernible coherence between tropical and subtropical signals. In contrast to their results, which used a more simplified chemistry scheme and fewer advected species, our model has reproduced the general pattern of the total ozone QBO in both the tropics and

subtropics with an apparent subtropical phase change between them in good agreement with observations.

[24] According to the conceptual model of the ozone QBO advanced by *Reed* [1964], during the equatorial westerly phase in the lower stratosphere, the atmospheric column is displaced downward with the descent of the westerly shear zone; since there is reduced tropical mean upwelling which prevents ozone-poor air from being advected upward from the lower stratosphere and hence results in an increase in total column ozone compared with the easterly phase. Thus the column ozone anomaly depends not only on the strength of the induced QBO circulation but also on the vertical gradient of the background ozone distribution, which increases with height in the lower stratosphere and peaks near 10 hPa (30–35 km). It is worth pointing out that for long-lived trace gases,

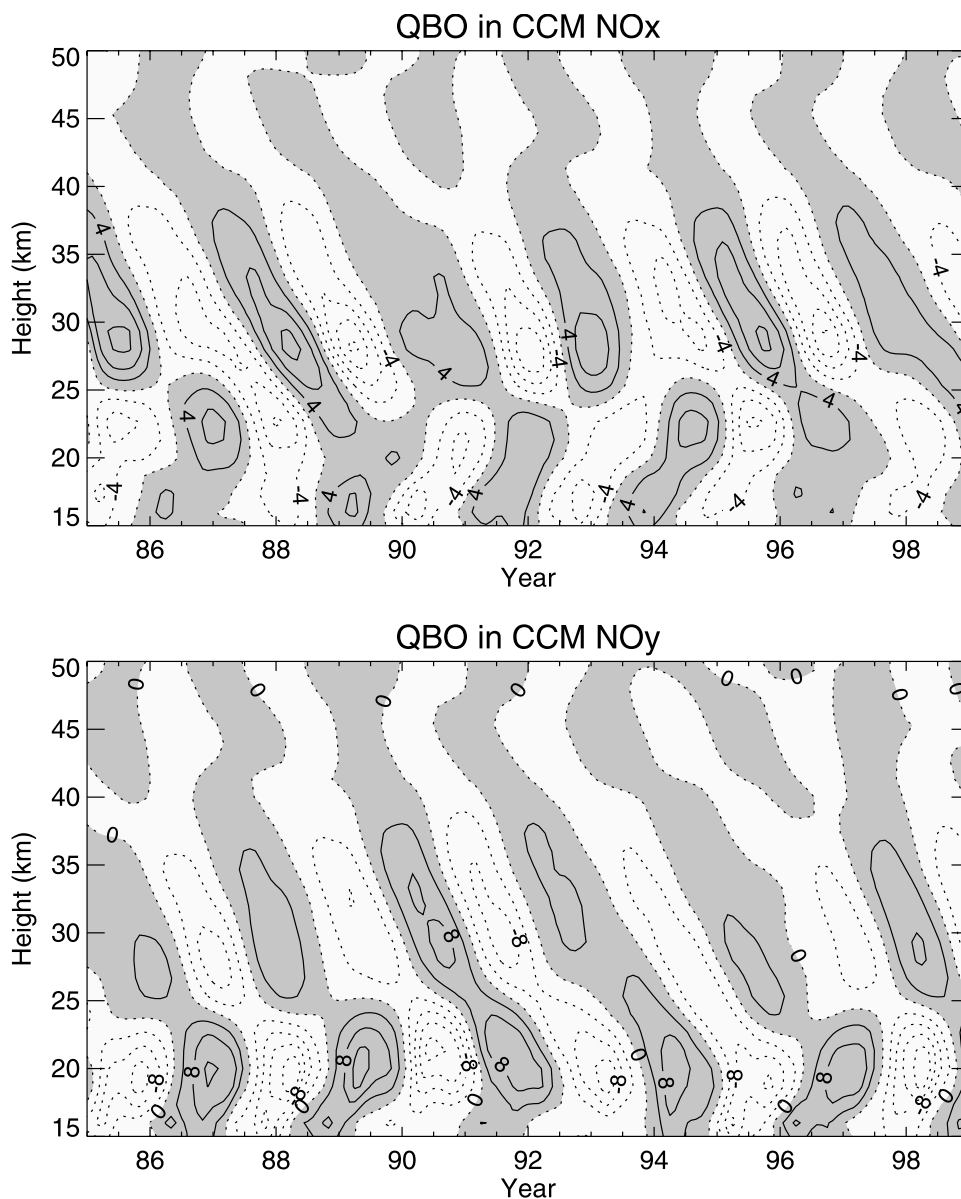


**Figure 9.** Height-time section of the percentage anomaly at the equator in the model (top)  $\text{NO}_x$  ( $= \text{NO} + \text{NO}_2$ ) and (bottom)  $\text{NO}_y$  fields. Contour interval is 4%.

for which chemical destruction/production can be neglected, no QBO signal can be generated by vertical transport if the tracer distribution is vertically uniform.

[25] The column ozone anomalies at high latitudes also reflect a modulation of the strength of the mean meridional circulation, although in this case it is a modulation arising from a change in planetary wave activity rather than a direct modulation by the QBO-induced meridional circulation. In an easterly QBO phase, the planetary wave activity is confined to middle and high latitudes by the presence of a zero wind line in the subtropics and the strength of the mean circulation is increased [Holton and Tan, 1980, 1982]. Similarly, when the QBO winds are westerly, the meridional circulation is weaker and hence there is less descent and reduced column ozone amounts at high latitudes [see, e.g., Hamilton, 1998].

[26] Gray and Pyle [1989] suggested that an additional important factor in determining the column ozone QBO at

high latitudes was the relatively sharp vertical gradient in the ozone chemical lifetime, which changes from days to months above 28 km to months to years below 28 km. They proposed that vertical advection of an ozone anomaly downward across this transition level by the large-scale mean meridional circulation into the region below 28 km would produce a significant column ozone anomaly because the atmosphere cannot respond quickly to remove the anomaly. While this is very likely to be an important factor at higher latitudes, we note that this is unlikely to be important in determining the equatorial column ozone anomalies, since the background circulation is always upward in this region.

## 6. Role of Chemistry in Driving the Ozone QBO

[27] In order to help understand the QBO signal in ozone in the region above  $\sim 28$  km where ozone has a relatively short lifetime, Figure 9 shows the time-height cross section of the

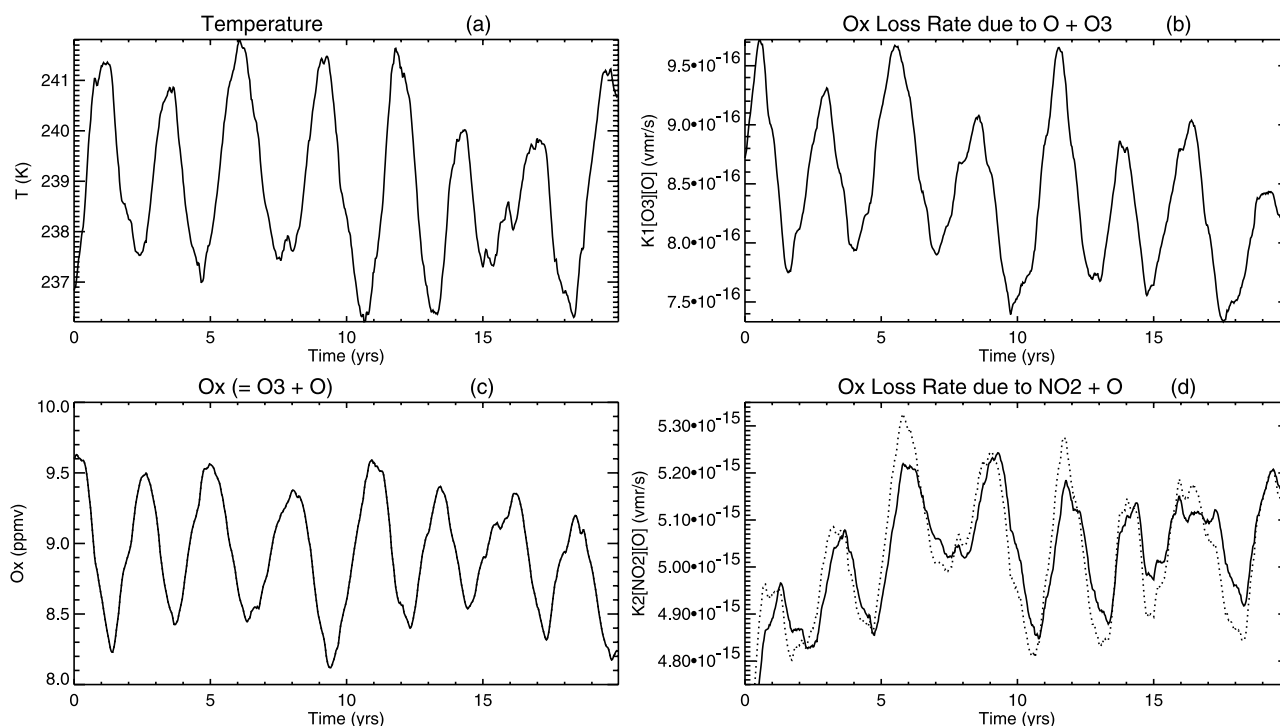


**Figure 10.** Results from a photochemical box model located at 35 km over the equator: (a) temperature (K), (b) second-order  $O_x$  loss rate (volume mixing ratio,  $s^{-1}$ ) due to  $O + O_3$  (i.e.,  $k_1[O_3][O]$ ), (c)  $O_x$  ( $=O_3 + O$ ), and (d) second-order  $O_x$  loss rate ( $s^{-1}$ ) due to  $NO_2 + O$  (i.e.,  $k_2[NO_2][O]$ ). Figure 10d also shows the sum of the two solid lines in Figures 10b and 10c (i.e., total  $O_x$  loss rate due to the two cycles) offset by the mean of the  $O + O_3$  cycle ( $8.44 \times 10^{-16} s^{-1}$ ). All plots have been smoothed with a 2-year running mean.

anomalies in the model  $NO_x$  ( $NO_2 + NO$ ) and total odd nitrogen ( $NO_y = N + NO + NO_2 + NO_3 + HNO_3 + 2N_2O_5 + ClONO_2 + BrONO_2 + HO_2NO_2$ ) fields at the equator, processed in the same way as  $O_3$ . Note that the model  $NO_2$  and  $NO$  are advected as a single tracer, and output is not saved at the same local time as the SAGE II observations. Therefore we cannot make a direct comparison between the model and SAGE II  $NO_2$  observations, but the overall structure of the QBO in the modelled  $NO_x$  and SAGE II  $NO_2$  is similar (not shown).

[28]  $NO_y$  is a long-lived tracer in the lower stratosphere with a lifetime of many years, although it is chemically removed in the upper stratosphere. In contrast the lifetime of  $NO_x$  in the middle to lower stratosphere is of the order of days. The vertical structure of the QBO in  $NO_y$  is similar to that in  $NO_x$  with an apparent phase change level at around 25 km (about 3 km lower than that for the ozone QBO). This suggests that the  $NO_x$  QBO is primarily determined by the variations in the total  $NO_y$ . However, the  $NO_y$  anomalies are stronger than  $NO_x$  anomalies in the lower stratosphere but weaker in the middle and upper stratosphere, indicating some changes in the chemical partitioning of  $NO_y$ . Also noticeable is that in the upper stratosphere at about 40 and 48 km there are two other visible phase changes in the  $NO_x$  and  $NO_y$  QBOs. The phase changes at  $\sim 25$  km in the  $NO_y$  (and  $NO_x$ ) QBO suggest that, in addition to the mechanism for the  $O_3$  phase change at  $\sim 28$  km proposed by *Gray and Pyle* [1989], dynamical processes may also play an important role. The long lifetime of  $NO_y$  means that it will not be subject to chemical modulation in generating its QBO, yet it also

displays a phase change at  $\sim 25$  km. The origin of this feature requires further investigation.

[29] As discussed in section 1, previous studies have reached conflicting conclusions on the role of  $NO_x$  variations, through transport of  $NO_x$ , in contributing to the  $O_3$  QBO above 28 km. Many studies have referred generally to the anticorrelation of the  $O_3$  and temperature QBOs, although *Chipperfield et al.* [1994] argued that the QBO in  $NO_x$  was an important factor. However, recently *Butchart et al.* [2003] obtained an  $O_3$  QBO in their CCM which did not include variations in long-lived tracer transport. To investigate this further we have used a photochemical box model to diagnose the CCM's  $O_3$  budget. The box model has an identical photochemical scheme to the 3D model and was initialized with CCM output every 10 days over a 20-year simulation. Results from the model at 35 km over the equator are given in Figure 10 which shows the time series of modelled odd oxygen ( $O_x = O_3 + O$ ) and the corresponding temperature QBO signals from the UM. Also shown are the second-order  $O_x$  loss rates for the  $O_3 + O$  and  $NO_2 + O$  cycles, i.e.,  $k_1[O_3][O]$  and  $k_2[NO_2][O]$ , respectively where  $k_1$  and  $k_2$  are the reaction rate constants. This altitude region is one where  $NO_x$  chemistry is known to dominate the loss of  $O_x$ . On average, the model  $NO_2 + O$  cycle is  $\sim 70\%$  of the total loss while the  $O_3 + O$  is  $\sim 10\%$ . This clearly shows the greater leverage for variations in  $NO_x$ -catalyzed loss to affect  $O_3$ . Variations in the rate of  $NO_x$ -catalyzed loss could occur through changes in  $[NO_x]$  itself or through the (weak) temperature-dependent rate constant (e.g., 1–2% change for 4K change in temperature). Ultimately, for  $O_3 + O$ ,

QBO-induced effects will be solely due to the fairly strong temperature dependence of this reaction (e.g., 17% change for 4K change in temperature). Figure 10b shows that the rate of  $k_1[\text{O}_3][\text{O}]$  varies by about  $\pm 7\%$  (i.e.,  $\pm 0.7\%$  of total  $\text{O}_x$  loss rate) and lags the  $\text{O}_3$  changes by about  $\pi/2$ . (Note that the temperature effect via  $k_1$  is out of phase with the dominant  $\text{O}_3$  signal, however). The rate of  $k_2[\text{NO}_2][\text{O}]$  varies by  $\pm 4\%$  (i.e.,  $\pm 2.8\%$  of total  $\text{O}_x$  loss rate) and lags the  $\text{O}_3$  signal by just under  $\pi/2$ . Figure 10d also includes the sum of the  $\text{O}_x$  loss due to these 2 cycles (dotted line), offset by the mean loss due to  $\text{O} + \text{O}_3$  (averaged over the whole time period) to aid comparison. This shift allows the relative phases and amplitudes of the 2 curves to be seen more easily and allows comparison of the QBO signal in  $\text{NO}_x$ -induced loss with that for the total loss due to  $\text{O}_x + \text{NO}_x$ . This illustrates the larger variation of loss due to  $\text{NO}_2$  but also shows the extra relative forcing due to the  $\text{O} + \text{O}_3$  cycle and its effect on the overall phase of the  $\text{O}_x$  loss. The phase of this overall loss rate tends to lag the  $\text{O}_3$  QBO by about  $\pi/2$  as expected. Therefore we conclude that the  $\text{NO}_x$  QBO does make a dominant chemical contribution to the  $\text{O}_3$  QBO in this region, in agreement with Chipperfield *et al.* [1994].

## 7. Summary and Conclusions

[30] We have used a fully coupled CCM to study QBO signals in stratospheric chemical species. The model is capable of generating spontaneous QBO-like oscillations in tropical wind and temperature as well as in a range of stratospheric chemical species advected by the CCM. This extends previous model studies, which have been limited either by the 2D framework or by more simplified chemical coupling in the 3D studies. We have found that the coupling of interactive chemistry affects the model QBO. For the 20 years of the model simulation, the wind QBO period increased by about 4 months and the Fourier QBO amplitude increased by  $1.5 \text{ m s}^{-1}$  in the middle and lower stratosphere due to the coupling.

[31] The basic properties and general features of QBO signals in wind, temperature, and chemical species generated by the model compare well with observations. For  $\text{O}_3$ , for which there are most observations, the model captures the general magnitude of the QBO signal and the altitude/latitudes of the observed phase changes. There are, however, two main discrepancies between modelled QBO signals and observed ones: First, the modelled QBO signals do not penetrate deep enough in the lower stratosphere, and second, the QBO signal in tropical ozone is relatively weaker than observed.

[32] From the CCM simulations, it is found that the QBO signals exist in many chemical species although we did not show all of them. Since the long-lived chemical species like  $\text{CH}_4$  and  $\text{N}_2\text{O}$  are not subject to significant chemical modulation, we can conclude that the QBO signals in chemical species are mainly caused by QBO-induced transport processes rather than chemical processes. Chemical processes clearly have a significant impact on the QBO signals in ozone and the diabatic effect of the ozone QBO can feed back and cause changes in the QBO amplitude and period. By diagnosing chemical rates from the model, we find that the model QBO in  $\text{NO}_2$ , itself largely caused by the QBO of the longer-lived  $\text{NO}_x$ , is the main chemical driver for the  $\text{O}_3$  QBO near 35 km, rather than temperature changes. However,

it is worth noting that the phase change in the ozone QBO at 28 km is also related to the QBO-induced transport. Our model simulations show that a phase change in height may not only exist in the ozone QBO signals but also in QBO signals of other long-lived chemical species.

[33] This study has demonstrated that current CCMs can reproduce an important aspect of middle atmosphere tracer variability. Whether the accurate representation of this variability is important for decadal-scale climate runs, will need further investigation.

[34] **Acknowledgments.** This research was supported by the EU SCOUT-O3 project. Computing support was provided by the NERC NCAS programme. The critical comments from three anonymous reviewers substantially improved the quality of the paper. We thank Stephen Arnold for proofreading the manuscript and for comments.

## References

- Baldwin, M. P., et al. (2001), The quasi-biennial oscillation, *Rev. Geophys.*, *39*, 179–229.
- Bruhwyler, L. P., and K. Hamilton (1999), A numerical simulation of the stratospheric ozone quasi-biennial oscillation using a comprehensive general circulation model, *J. Geophys. Res.*, *104*, 30,525–30,557.
- Butchart, N., A. A. Scaife, J. Austin, S. H. E. Hare, and J. R. Knight (2003), Quasi-biennial oscillation in ozone in a coupled chemistry-climate model, *J. Geophys. Res.*, *109*(D15), 4486, doi:10.1029/2002JD003004.
- Chipperfield, M. P. (1999), Multiannual simulations with a three-dimensional chemical transport model, *J. Geophys. Res.*, *104*, 1781–1805.
- Chipperfield, M. P., and L. J. Gray (1992), Two-dimensional model studies of interannual variability of trace gases in the middle atmosphere, *J. Geophys. Res.*, *97*, 5963–5980.
- Chipperfield, M. P., L. J. Gray, J. S. Kinnersley, and J. Zawodny (1994), A two-dimensional model study of QBO signal in SAGE II  $\text{NO}_2$  and  $\text{O}_3$ , *Geophys. Res. Lett.*, *21*, 589–592.
- Cullen, M. J. P. (1993), The unified forecast/climate model, *Meteorol. Mag.*, *122*, 81–94.
- Gates, W. L., et al. (1999), An overview of the results of the Atmospheric Model Intercomparison Project (AMIP I), *Bull. Am. Meteorol. Soc.*, *80*(1), 29–56.
- Gray, L. J., and M. P. Chipperfield (1990), On the interannual variability of trace gases in the middle atmosphere, *Geophys. Res. Lett.*, *17*, 933–936.
- Gray, L. J., and J. A. Pyle (1989), A two dimensional model of the quasi-biennial oscillation of ozone, *J. Atmos. Sci.*, *46*, 203–220.
- Gray, L. J., S. J. Phipps, T. J. Dunkerton, M. P. Baldwin, E. F. Drysdale, and M. R. Allen (2001), A data study of the influence of the equatorial upper stratosphere on northern hemisphere stratosphere sudden warmings, *Q.J.R. Meteorol. Soc.*, *127*, 1985–2003.
- Hamilton, K. (1998), Effects of an imposed quasi-biennial oscillation in a comprehensive troposphere-stratosphere-mesosphere general circulation model, *J. Atmos. Sci.*, *55*, 2393–2418.
- Hasebe, F. (1994), Quasi-biennial oscillation of ozone and diabatic circulation in the equatorial stratosphere, *J. Atmos. Sci.*, *51*, 729–754.
- Holton, J. R., and H.-C. Tan (1980), The influence of the equatorial quasi-biennial oscillation on the global circulation at 50 mb., *J. Atmos. Sci.*, *37*, 2200–2208.
- Holton, J. R., and H.-C. Tan (1982), The quasi-biennial oscillation in the Northern Hemisphere lower stratosphere, *J. Meteorol. Soc. Jpn.*, *60*, 140–148.
- Huang, T. Y. W. (1996), The impact of solar radiation on the quasi-biennial oscillation of ozone in the tropical stratosphere, *Geophys. Res. Lett.*, *23*, 3211–3214.
- Li, D., K. P. Shine, and L. J. Gray (1995), The role of ozone-induced heating anomalies in the quasi-biennial oscillation, *Q.J.R. Meteorol. Soc.*, *121*, 937–943.
- Ling, X. D., and J. London (1986), The quasi-biennial oscillation of ozone in the tropical middle stratosphere: A one-dimensional model, *J. Atmos. Sci.*, *43*, 3122–3137.
- Nagashima, T., M. Takahashi, and F. Hasebe (1998), The first simulation of an ozone QBO in a general circulation model, *Geophys. Res. Lett.*, *25*, 3131–3134.
- Pascoe, C., L. J. Gray, S. A. Crooks, M. N. Juckes, and M. P. Baldwin (2005), The quasi-biennial oscillation: Analysis using ERA-40 data, *J. Geophys. Res.*, *110*(D8), D08105, doi:10.1029/2004JD004941.
- Randel, W. J., and F. Wu (1996), Isolation of the ozone QBO in SAGE II data by singular value decomposition, *J. Atmos. Sci.*, *53*, 2546–2559.

- Reed, R. J. (1964), A tentative model of the 26 month oscillation in tropical latitudes, *Q.J.R. Meteorol. Soc.*, *105*, 441–466.
- Scaife, A., N. Butchart, C. D. Warner, D. Stainforth, W. Norton, and J. Austin (2000), Realistic quasi-biennial oscillation in a simulation of global climate, *Geophys. Res. Lett.*, *27*, 3481–3484.
- Scaife, A., N. Butchart, C. D. Warner, and R. Swinbank (2002), Impact of a spectral gravity wave parameterization on the stratosphere in the Met Office Unified Model, *J. Atmos. Sci.*, *59*, 1473–1489.
- Swinbank, R., et al. (1998), Middle atmospheric variability in the UK Meteorological Office Unified Model, *Q.J.R. Meteorol. Soc.*, *125*, 1485–1525.
- Tian, W., and M. P. Chipperfield (2005), A new coupled chemistry-climate model for the stratosphere: The importance of coupling for future O<sub>3</sub>-climate predictions, *Q.J.R. Meteorol. Soc.*, *131*, 281–303.
- Warner, C. D., and M. E. McIntyre (1999), Towards an ultra-simple spectral gravity wave parameterisation for general circulation models, *Earth Planets Space*, *51*, 475–485.
- World Meteorological Organization (2003), Scientific assessment of ozone depletion: 2002, Global Ozone Research and Monitoring Project, *Rep. 47*, 498 pp., Geneva, Switzerland.
- Zawodny, J., and M. P. McCormick (1991), Stratospheric aerosol and gas experiment II measurements of the quasi-biennial oscillation in ozone and nitrogen dioxide, *J. Geophys. Res.*, *96*, 9371–9377.

---

M. P. Chipperfield and W. Tian, Institute for Atmospheric Science, School of Earth and Environment, University of Leeds, Leeds LS2 9JT, UK. (wenshou@env.leeds.ac.uk)

L. J. Gray, Centre for Global Atmospheric Modeling, Department of Meteorology, University of Reading, Earley Gate, P. O. Box 243, Reading RG6 6BB, UK.

J. M. Zawodny, NASA Langley Research Center, Mail Stop 475, Hampton, VA 23681-0001, USA.